Supporting Information for

Direct Measurements of Unimolecular and Bimolecular Reaction Kinetics of the Criegee Intermediate $(CH_3)_2COO$

Rabi Chhantyal-Pun, Oliver Welz, John D. Savee, Arkke J. Eskola, Edmond P. F. Lee, Lucy Blacker, Henry R. Hill, Matilda Ashcroft, M. Anwar H. Khan, Guy C. Lloyd-Jones, Louise Evans, Brandon Rotavera, Haifeng Huang, David L. Osborn, Daniel K. W. Mok, John M. Dyke, Dudley E. Shallcross, Carl J. Percival, Andrew J. Orr-Ewing, and Craig A. Taatjes

Complete references from main manuscript:

8. Taatjes, C. A.; Welz, O.; Eskola, A. J.; Savee, J. D.; Scheer, A. M.; Shallcross, D. E.; Rotavera, B.; Lee, E. P. F.; Dyke, J. M.; Mok, D. K. W.; Osborn, D. L.; Percival, C. J., Direct Measurements of Conformer-Dependent Reactivity of the Criegee Intermediate CH_3CHOO. *Science* **2013**, *340*, 171-180.

16. Sipilä, M.; Jokinen, T.; Berndt, T.; Richters, S.; Makkonen, R.; Donahue, N. M.; Mauldin III, R. L.; Kurten, T.; Paasonen, P.; Sarnela, N.; Ehn, M.; Junninen, H.; Rissanen, M. P.; Thornton, J.; Stratmann, F.; Herrmann, H.; Worsnop, D. R.; Kulmala, M.; Kerminen, V.-M.; Petäjä, T., Reactivity of Stabilized Criegee Intermediates (sCIs) from Isoprene and Monoterpene Ozonolysis toward SO_2 and Organic Acids. *Atmos. Chem. Phys.* **2014**, *14*, 12143−12153.

17. Welz, O.; Eskola, A. J.; Sheps, L.; Rotavera, B.; Savee, J. D.; Scheer, A. M.; Osborn, D. L.; Lowe, D.; Booth, A. M.; Xiao, P.; Khan, M. A. H.; Percival, C. J.; Shallcross, D. E.; Taatjes, C. A., Rate Coefficients of C1 and C2 Criegee Intermediate Reactions with Formic and Acetic Acid Near the Collision Limit: Direct Kinetics Measurements and Atmospheric Implications. *Angew. Chem. Int. Ed.* **2014,** *53*, 4547–4550.

23. Frisch, M. J.; Trucks, G. W.; Schlegel, H. B.; Scuseria, G. E.; Robb, M. A.; Cheeseman, J. R.; Scalmani, G.; Barone, V.; Mennucci, B.; Petersson, G. A.; Nakatsuji, H.; Caricato, M.; Li, X.; Hratchian, H. P.; Izmaylov, A. F.; Bloino, J.; Zheng, G.; Sonnenberg, J. L.; Hada, M.; Ehara, M.; Toyota, K.; Fukuda, R.; Hasegawa, J.; Ishida, M.; Nakajima, T.; Honda, Y.; Kitao, O.; Nakai, H.; Vreven, T.; Montgomery, J., J. A.; Peralta, J. E.; Ogliaro, F.; Bearpark, M.; Heyd, J. J.; Brothers, E.; Kudin, K. N.; Staroverov, V. N.; Kobayashi, R.; Normand, J.; Raghavachari, K.; Rendell, A.; Burant, J. C.; Iyengar, S. S.; Tomasi, J.; Cossi, M.; Rega, N.; Millam, N. J.; Klene, M.; Knox, J. E.; Cross, J. B.; Bakken, V.; Adamo, C.; Jaramillo, J.; Gomperts, R.; Stratmann, R. E.; Yazyev, O.; Austin, A. J.; Cammi, R.; Pomelli, C.; Ochterski, J. W.; Martin, R. L.; Morokuma, K.; Zakrzewski, V. G.; Voth, G. A.; Salvador, P.; Dannenberg, J. J.; Dapprich, S.; Daniels, A. D.; Farkas, Ö.; Foresman, J. B.; Ortiz, J. V.; Cioslowski, J.; Fox, D. J. *Gaussian 09, Revision A.02*, Gaussian, Inc.: Wallingford CT, 2009.

24. Werner, H.-J.; Knowles, P. J.; Manby, F. R.; Schütz, M.; Celani, P.; Knizia, G.; Korona, T.; Lindh, R.; Mitrushenkov, A.; Rauhut, G.; Adler, T. B.; Amos, R. D.; Bernhardsson, A.; Berning, A.; Cooper, D. L.; Deegan, M. J. O.; Dobbyn, A. J.; Eckert, F.; Goll, E.; Hampel, C.; Hesselmann, A.; Hetzer, G.; Hrenar, T.; Jansen, G.; Köppl, C.; Liu, Y.; Lloyd, A. W.; Mata, R. A.; May, A. J.; McNicholas, S. J.; Meyer, W.; Mura, M. E.; Nicklass, A.; Palmieri, P.; Pflüger, K.; Pitzer, R.; Reiher, M.; Shiozaki, T.; Stoll, H.; Stone, A. J.; Tarroni, R.; Thorsteinsson, T.; Wang, M.; Wolf, A. *MOLPRO, version 2012.1, a package of ab initio programs (see http://www.molpro.net).* 2012.

Calculation Details

Ionization energies of $(CH_3)_2COO$, $CH_2=C(CH_3)OOH$, 3-methyl-1,2-dioxetane and dimethyl-dioxirane, and Franck-Condon factors of the ionizations

As described in the text, after a DFT survey, higher level energy calculations were carried out at the B3LYP/6-311++G** geometries employing the explicit correlation methods, RHF/UCCSD(T)-F12x, x = a or b,[1] as installed in MOLPRO2012.[2] The scaled

perturbative triples, obtained by a simple scaling factor, $\Delta E(T_{sc}) = \Delta E(T)$ x E_{corr}^{MP2}-F12/E_{corr}^{MP2} (i.e. the ratio between the computed correlation energies obtained at the MP2 and MP2-F12 levels) were used throughout. The cc-pVXZ-F12[3] and cc-pVXZ-F12_OPTRI[4-5] basis sets, where X = T or Q, which were designed specifically for F12 calculations, were used in the AO (atomic orbital) and RI (resolution of identity, or CABS, complementary auxiliary basis sets) basis sets, respectively, in these F12 calculations, together with the corresponding aug-cc-pVXZ_MP2FIT basis sets[6] in the DF (density fitting) basis set.

Franck-Condon factors (FCFs) between the $\tilde{X}^1A'$ state of $(CH_3)_2COO$ and the two lowest electronic states, $^2A''$ and $^2A'$, of its cation were computed within the harmonic oscillator model, with allowance for Duschinsky rotation, using the EZSPECTRUM code.[7] The two sets of geometries, harmonic vibrational frequencies and normal mode vectors obtained at the B3LYP/6-311++G** and M06-2X/AVDZ levels were used in the FCF calculations.

For $CH_2=C(CH_3)OOH$, 3-methyl-1,2-dioxetane and dimethyl-dioxirane (and their cations), isomers of $(CH_3)_2COO$, geometry optimization and harmonic vibrational frequency calculations were performed at the B3LYP/6-311++G** level. Improved relative electronic energies for $CH_2=C(CH_3)OOH$ were computed at the RHF/UCCSD(T)-F12x/CBS level, similar to $(CH_3)_2COO$ described above. For both $(CH_3)_2COO$ and $CH_2=C(CH_3)OOH$, it was found that the computed UCCSD(T)-F12a and UCCSD(T)-F12b IE values using the VTZ-F12 and VQZ-F12 basis sets converge to the CBS limit values from opposite directions (*vide infra*). As a result, the averages between the F12a and F12b values, whether with the VTZ-F12 or VQZ-F12 basis set, are very close to the CBS values. In view of this finding, for 3-methyl-1,2-dioxetane and dimethyl-dioxirane, ionization energies were computed only at the UCCSD(T)-F12x/cc-pVTZ-F12 level, and the averages of the F12a and F12b values were taken to be the best theoretical values and were used in subsequent FCF calculations. FCFs for the first photoelectron ionization band of all these species were computed within the harmonic oscillator model, with allowance for Duschinsky rotation. For the dimethyl-dioxirane cations, low-lying cationic states were investigated at the M06-2X/6-311++G**, TD-B3LYP/6-311++G** and CASSCF(8,8)/NEVPT2/aug-cc-pVDZ levels, in order to establish the ground cationic state. TD-B3LYP calculations were performed using GAUSSIAN09,[8] and CASSCF/NEVPT2 calculations with MOLPRO2012.[2]

Reaction energy profiles of reactions 1 and 2:
$(CH_3)_2CI + O_2 \rightarrow (CH_3)_2CIOO$ …. Reaction 1
$(CH_3)_2CIOO \rightarrow (CH_3)_2COO + I$ …. Reaction 2

The higher level *ab initio* energy calculations at M06-2X stationary points on the reaction energy surfaces included single-reference (SR) methods, namely RHF/UCCSD(T) [9] and RHF/UCCSD(T)-F12x, and multi-reference (MR) methods, namely, CASSCF, CASSCF/NEVPT2, CASSCF/CASPT2 and CASSCF/CASPT2-F12. MR methods were used mainly for the TS of reaction 2 (and $(CH_3)_2CIOO$ in order to obtain the relative electronic energy; *vide infra*) because the computed T1 diagnostics obtained from UCCSD calculations on the TS have values of *ca*. 0.068, which suggest some MR character. Nevertheless, computed CASSCF wavefunctions of the TS show only very small configuration interaction (CI), as the two largest computed CI coefficients are 0.978 and -0.187 (*vide infra*). CASSCF calculations have employed an active space of 3 electrons in 4 molecular orbitals (*i.e.* CASSCF(3,4)). The post-CASSCF NEVPT2 and CASPT2 methods, as implemented in MOLPRO2012, are two variants of second-order MR perturbation theory (MR-PT2). The NEVPT2 (n-electron valence state perturbation theory) method[10-12] has a main advantage over other MR-PT2 methods in the absence of intruder states. The CASPT2 method in MOLPRO is based on the Rayleigh Schrodinger perturbation theory,[13] and has been extended

very recently to combine with F12 explicitly correlation theory to give the CASPT2-F12 method.[14] The AO basis sets used in these higher level *ab initio* calculations are aug-cc-pVXZ (for C, O and H) and aug-cc-PVXZ-PP (and associated ECP28MDF for I) basis sets, where X = D or T (denoted by AVDZ or AVTZ for simplicity). For F12 calculations, the corresponding aug-cc-pXZ_OPTRI[5] and aug-cc-pVXZ_MP2FIT[6] basis sets were used for C, O and H in the RI and DF basis sets, respectively. For I, the s, p and d functions of the def2-ASVP-MP2FIT and def2-SVP-OPT basis sets[15-17] were used in the DF and RI basis sets, with the AVDZ quality AO basis set, while the s, p, d and f functions of the def2-ATZVPP-MP2FIT and def2-TZVPP-OPT basis sets were used with the AVTZ quality AO basis set. In some cases, extrapolation to the CBS limit was also carried out using the $1/X^3$ formula, as described above.

Detailed quantum chemistry results

The $\tilde{X}^1A'$ state of $(CH_3)_2COO$ and the $\tilde{X}^2A''$ and $\tilde{A}^2A'$ states of $(CH_3)_2COO^+$

Some optimized geometrical parameters, computed harmonic vibrational frequencies and ionization energies (adiabatic and vertical, AIE and VIE) obtained at the B3LYP/6-311++G** and M06-2X/AVDZ levels of calculation are summarized in Table S1. Computed relative electronic energies obtained at higher *ab initio* levels are given in Table S2. Considering the computed higher level results given in Table S2, first, it can be seen that the computed UCCSD(T)-F12a and UCCSD(T)-F12b AIE and VIE values obtained using the VTZ-F12 and VQZ-F12 basis sets converge to the CBS limit values from opposite directions as mentioned above. Second, it is pleasing that the differences between the F12a/CBS and F12b/CBS values are smaller than 0.01 eV in all cases. Third, the averages of the F12a and F12b values obtained using both the VTZ-F12 and VQZ-F12 basis sets are very close to the CBS values (within 0.01 eV). In this connection, the averages of the F12a/VTZ-F12 and F12b/VTZ-T12 values can be considered as reliable estimates as mentioned above. Summing up, the best computed AIE and VIE values obtained here are highly reliable with estimated uncertainties of within 0.01 eV.

Computed FCFs for ionization from the $\tilde{X}^1A'$ state of $(CH_3)_2COO$ to the two lowest cation states are shown as bar diagrams in Figures S1 and S2. FCFs were computed using both sets of B3LYP and M06-2X geometries and vibrational frequencies (upper and lower bar diagrams in Figures S1 and S2).

The $\tilde{X}^1A$ state of $CH_2=C(CH_3)OOH$ and the $\tilde{X}^2A''$ state of $CH_2=C(CH_3)OOH^+$

Some optimized geometrical parameters, computed harmonic vibrational frequencies and ionization energies (AIE and VIE) obtained at the B3LYP/6-311++G** level of calculation are summarized in Table S3. The ground electronic state of $CH_2=C(CH_3)OOH$ was optimized to a C_1 structure, with H of the OH group out of the $(C_2)COO$ plane, while the ground electronic state of the cation has C_S symmetry (a $^2A''$ state) with the OH group in plane. In addition, the CH_3 groups in the neutral molecule and the cation have different orientations. Specifically, the neutral molecule has the HCCO dihedral angle of a methyl hydrogen equalled to 180.0 degrees, while the cation has HCCO = 0.0 degree (*i.e.* rotation of the methyl group by ~60 degrees). The neutral molecule with C_S symmetry (OH in plane) and the CH_3 group with the same orientation as in the C_1 minimum is a first order saddle point, with one computed imaginary frequency (148i cm^{-1}) of the a″ OH wagging mode. This first order saddle point is only 0.19 $kcal.mol^{-1}$ higher in energy than the C_1 minimum at the B3LYP/6-311++G** level of calculation, suggesting a free OH rotation. The neutral molecule with C_S symmetry (OH in plane) and the CH_3 group with the same orientation as in the cation is a second order saddle point (see Table S3, under neutral $^1A'$). The two vibration

modes with computed imaginary frequencies (170i and 147i cm^{-1}) are essentially the CH_3 torsional and OH wagging modes. This second order saddle point was computed to be ~2.0 $kcal.mol^{-1}$ higher in energy than the true minimum (see Table S3), suggesting that the two imaginary modes are essentially free rotations.

The lowest cationic state of CH_2=C(CH_3)OOH^+ is the $\tilde{X}^2A''$ state. B3LYP calculations on the lowest $^2A'$ state converged to the $^2A''$ state. Further TD-B3LYP/6-311++G** calculations were carried out to characterize the lowest $^2A'$ state. First, at the C_1 geometry of the neutral $\tilde{X}^1A$ state, the first excited state of the cation is 2.06 eV above the lowest state. Geometry optimization of the first excited state of the cation by TD-B3LYP calculation led to SCF convergence failure of the neutral state after 20 points. At this geometry, the OH group has moved out of the (C_2)CO plane. Second, at the C_S geometry of the $\tilde{X}^2A''$ state of the cation, TD-B3LYP calculations gave a $(2)^2A''$ state as the first excited state (with a computed excitation energy of 1.93 eV) and a $(1)^2A'$ state as the second excited state (with a computed excitation energy of 3.81 eV) of the cation. The geometry of the second excited state, $(1)^2A'$ state, was optimized, and at its optimized geometry, it has an estimated IE of 11.65 eV based on computed B3LYP energies and TD-B3LYP excitation energy. Summarizing, the lowest $^2A'$ state is significantly higher in energy than the $\tilde{X}^2A''$ state (AIE = 8.56 eV at the B3LYP level; see Table S3) and hence will be ignored from here onward.

Computed IEs to the $\tilde{X}^2A''$ state of CH_2=C(CH_3)OOH^+ obtained at higher levels of calculations are also given in Table S3. The best theoretical estimates of the AIE and AIE_0 values are 8.78 and 8.75 eV, respectively (see footnotes c and d of Table S3). The best computed AIE_0 value to the $\tilde{X}^2A''$ state of CH_2=C(CH_3)OOH^+ is 0.04 eV lower than the best computed AIE_0 value to $\tilde{X}^2A''$ state of $(CH_3)_2COO^+$. Computed FCFs for the ionization from the $^1A'$ state of CH_2=C(CH_3)OOH (second order saddle point) to the $\tilde{X}^2A''$ state of CH_2=C(CH_3)OOH^+ are shown as bar diagrams in Figure S3. The optimized geometry and computed harmonic vibrational frequencies (ignoring the two imaginary modes) of the second order saddle point of the neutral molecule (the $^1A'$ state discussed above) have been used in the FCF calculations instead of those of the true minimum (the C_1 $\tilde{X}^1A$ state), because the harmonic oscillator model cannot handle properly the OH wagging and CH_3 torsional modes, which are essentially free rotations, as discussed above. The computed FCFs (bar diagrams) shown in Figure S3 suggest that the first photoelectron band of CH_2=C(CH_3)OOH has a strong adiabatic vibrational component and extends to ~9.6 eV. The overall vibrational band envelope is quite different from the ionizations from the $\tilde{X}^1A'$ state of $(CH_3)_2COO$ to the $\tilde{X}^2A''$ and $\tilde{A}^2A'$ states of $(CH_3)_2COO^+$ as shown in Figures S1 and S2.

Energy profiles of reactions 1 and 2

Results obtained from M06-2X/AVDZ geometry optimization calculations are summarized as follows. The ground electronic state of $(CH_3)_2CI$ is a $^2A'$ state. It has a C_S structure with a mirror plane through CI (C_2CI not planar; the two methyl groups are mirror images of each other). The lowest $^2A''$ state is a first order saddle point with one a″ imaginary vibrational frequency (161i cm^{-1}), and is slightly higher in energy than the $^2A'$ state (by 1.0 $kcal.mol^{-1}$). This saddle point has a C_2CI mirror plane. For the sake of simplicity, only the $\tilde{X}^2A'$ state is considered from here onward. The ground electronic state of $(CH_3)_2CIOO$ has a C_1 structure. A conformer, a $^2A''$ state of C_S structure (with a mirror plane through ICOO), is 0.9 $kcal.mol^{-1}$ higher in energy than the C_1 lowest energy conformer. Also for the sake of simplicity, only the lowest energy C_1 conformer is considered.

Regarding TS searches, no TS was found for reaction 1. A relaxed energy scan of the C-O bond length at the M06-2X/AVDZ level shows only a small energy barrier of 0.02 $kcal.mol^{-1}$ at r(CO) = 2.35 Å with respect to the reactant complex at R(CO) = 2.55 Å, and an

overall negative energy barrier of -3.4 kcal.mol^{-1} with respect to separate reactants. Based on the relaxed energy scan, it is concluded that reaction 1 is effectively barrierless. For reaction 2, a TS was located. Computed relative energies at higher levels of calculation for both reactions 1 and 2 are summarized in Table S4. It should be noted that for ΔE_e^{RX} of reaction 2, spin-orbit contributions to I has been included (see footnote c of Table S4). Summing up, reaction 1 is barrierless and exothermic (ΔH_{298K} = -31.7 kcal.mol^{-1} at the highest level of calculation), while reaction 2 has a computed barrier of ~22 kcal.mol^{-1} (the average of F12a and F12b values = 22.5 kcal.mol^{-1} and the NEVPT2/CBS value = 22.1 kcal.mol^{-1}; Table S4), but is endothermic (ΔH_{298K} = 16.9 kcal.mol^{-1}). However, since reaction 1 is quite exothermic, excess energy from reaction 1 is more than sufficient to overcome the barrier of reaction 2 (the TS of reaction 2 is ~8.6 kcal.mol^{-1} below the reactant entrance energy). The computed overall enthalpy change at 298 K for the combined reactions 1 and 2 is -14.8 kcal.mol^{-1} (using computed ΔH_{298K} values of reactions 1 and 2 given in Table S4).

Comparing with analogous reactions for the formation of CH_2OO, the lightest member of Criegee intermediates, from $CH_2I + O_2$ studied previously,[18] the calculated reaction energy profiles of the formation of CH_2OO and $(CH_3)_2COO$ are quite different. Specifically, with CH_2OO, the analogous reaction 1 has a small computed barrier of 1.02 kcal.mol^{-1} (at the highest level of calculation[18]) and the analogous reaction 2 does not have a barrier. In contrast, with $(CH_3)_2COO$, reaction 1 is barrierless, but reaction 2 has a significant barrier, as discussed above. Also, the computed enthalpy changes of the overall reactions at 298 K (*i.e.* reactions 1 + 2) of $CY_2I + O_2 \rightarrow CY_2OO + I$, are -1.08 (at the RCCSD(T)/CBS level[18]) and -14.8 kcal.mol^{-1} (given above) for Y = H and CH_3, respectively, indicating that the formation of $(CH_3)_2COO$ is significantly more exothermic than the formation of CH_2OO. Regarding the bottleneck of the combined reactions 1 + 2, the formation of CH_2OO has a small computed barrier of 1.02 kcal.mol^{-1}, but the computed energy profile for the formation of $(CH_3)_2COO$ shows that all stationary points are below the reactant entrance energy. Summarizing, based on the computed reaction energy profiles of the two sets of reactions, the formation of $(CH_3)_2COO$ is expected to be more favourable than the formation of CH_2OO both kinetically and thermodynamically via the same sequence of reactions 1 and 2. However, CH_2OO is expected to be formed vibrationally cooler than $(CH_3)_2COO$.

Computed results of 3-methyl-1,2-dioxetane and dimethyl-dioxirane

Computed results of 3-methyl-1,2-dioxetane and dimethyl-dioxirane are summarized in Tables S5 and S6, respectively. For dimethyl-dioxirane, results of calculations on some low-lying excited cationic states are also given in Table S6. It can be seen from Table S6 that the ground electronic state of dimethyl-dioxirane is a $^2A_2$ state. The best computed AIE_0 values of the first ionization of 3-methyl-1,2-dioxetane and dimethyl-dioxirane are 9.12 and 9.91 eV (Tables S5 and S6) respectively. These values were used in FCF calculations. The computed FCFs are shown as bar diagrams in Figures S4 and S5. From the computed FCFs, the first ionization band of 3-methyl-1,2-dioxetane has a complex vibrational structure (Figure S4). The major vibrational progressions are the 14a and 27a modes with computed frequencies of 171 and 1176 cm^{-1}, which are essentially the methyl-ring wagging mode and bond stretches in the CCOO four-membered ring. These progressions are consistent with the computed geometry changes upon ionization. Specifically, the C_1O_1, C_2O_2 and O_1O_2 bond lengths change from 1.450, 1.462 and 1.488 Å in the neutral to 1.526, 1.480 and 1.337 Å in the cation, respectively. This ionization band covers the 9.1 to 10.1 eV IE region. As for the $\tilde{X}^2A_2 \leftarrow \tilde{X}^1A_1$ ionization of dimethyl-dioxirane, it has an even more complex vibrational structure than 3-methyl-1,2-dioxetane (Figure S5) and covers the 9.9 to 11.2 eV IE region. The highest doubly occupied $2a_2$ molecular orbital of dimethyl-dioxirane is essentially an OO π antibonding orbital. The ionization of an electron from this molecular orbital leads to

significant geometry changes. Specifically, the CC, CO and OO bond lengths change from 1.506, 1.402 and 1.501 Å in the neutral to 1.479, 1.494 and 1.330 Å in the cation. In the FCF calculation of this ionization, the total number of excitations considered in all normal modes combined in the cationic state is 9 and the maximum number of combination bands considered is 2,636,011,840.

*Table S1. Optimized geometrical parameters (bond lengths in Å and angle in degrees), computed harmonic vibrational frequencies (in cm^{-1}) of the $\widetilde{X}^1A'$ state of $(CH_3)_2COO$ and the lowest $^2A''$ and $^2A'$ states of $(CH_3)_2COO^+$ and the computed adiabatic (AIE) and vertical (VIE) ionization energies (in eV) obtained at the B3LYP/6-311++G** and M06-2X/AVDZ[a] levels of calculation.*

B3LYP	$\widetilde{X}^1A'$	$^2A''$	$^2A'$
C_1C_2;C_2C_3	1.489; 1.476	1.458; 1.460	1.469; 1.470
CO	1.267	1.321	1.288
OO	1.383	1.357	1.368
COO	117.8	115.4	119.0
CCC	124.5	125.6	126.0
Vib. freq.	154.0(a″), 177.4(a″), 274.9(a″), 306.3(a′), 362.8(a′), 477.1(a″), 596.7(a′), 812.2(a′), 910.5(a′), 932.3(a″), 984.0(a′), 1067.6(a′), 1089.0(a″), 1306.3(a′), 1393.4(a′), 1408.7(a′), 1437.4(a″), 1456.5(a′), 1468.8(a″), 1477.3(a′), 1556.4(a′), 3019.0(a′), 3023.7(a′), 3061.4(a″), 3068.2(a″), 3136.0(a′), 3138.5(a′)	25.0(a″), 125.9(a″), 217.9(a″), 330.3(a′), 389.4(a′), 493.7(a″), 594.6(a′), 817.3(a′), 838.9(a″), 964.2(a′), 995.2(a′), 1003.8(a′), 1048.6(a″), 1276.2(a′), 1327.6(a′), 1353.0(a′), 1402.4(a′), 1414.0(a″), 1420.6(a″), 1476.3(a′), 1487.3(a′), 2989.3(a′), 3009.5(a′), 3025.8(a″), 3044.0(a″), 3159.6(a′), 3165.4(a′)	114.8(a″), 159.1(a″), 253.8(a′), 296.4(a″), 373.6(a′), 509.2(a″), 559.0(a′), 785.8(a′), 893.0(a″), 903.3(a′), 983.9(a′), 1068.3(a′), 1110.4(a″), 1308.8(a′), 1353.4(a′), 1370.8(a′), 1430.2(a′), 1431.3(a″), 1463.2(a″), 1475.0(a′), 1499.5(a′), 2995.9(a′), 3012.2(a′), 3044.3(a″), 3058.4(a″), 3158.1(a′), 3165.7(a′)
AIE(VIE)		8.72 (8.99)	8.87 (9.00)
M062X			
C_1C_2;C_2C_3	1.488; 1.475	1.458; 1.461	1.468; 1.470
CO	1.257	1.313	1.282
OO	1.366	1.339	1.357
COO	116.8	114.6	116.5
CCC	124.4	125.4	125.9
Vib. freq.	169.7(a″), 212.9(a″), 290.8(a″), 330.4(a′), 362.9(a′), 483.9(a″), 616.0(a′), 830.4(a′), 908.4(a″), 956.2(a′), 979.0(a′), 1075.6(a′), 1083.2(a″), 1306.6(a′), 1369.7(a′), 1390.5(a′), 1414.3(a″), 1442.6(a′), 1446.3(a″), 1474.6(a′), 1648.0(a′), 3059.4(a′), 3066.4(a′), 3118.3(a″), 3132.8(a″), 3190.3(a′), 3194.8(a′)	74.7(a″), 141.8(a″), 225.9(a″), 348.6(a′), 391.0(a′), 477.6(a″), 612.8(a′), 819.1(a″), 834.6(a′), 967.8(a′), 1012.9(a′), 1029.(a″), 1068.7(a′), 1291.9(a′), 1311.6(a′), 1335.9(a′), 1399.3(a″), 1405.0(a″), 1411.3(a′), 1487.4(a′), 1491.9(a′), 3024.8(a′), 3042.4(a′), 3079.9(a″), 3095.6(a″), 3206.2(a′), 3213.3(a′)	129.6(a″), 174.9(a″), 280.0(a′), 296.9(a″), 374.1(a′), 500.5(a″), 574.7(a′), 817.1(a′), 867.8(a″), 959.0(a′), 985.2(a′), 1082.7(a′), 1112.2(a″), 1323.6(a′), 1336.3(a′), 1356.3(a′), 1412.7(a″), 1426.0(a′), 142.2(a″), 1473.1(a′), 1561.1(a′), 3027.1(a′), 3046.2(a′), 3091.7(a″), 3109.8(a″), 3206.4(a′), 3211.9(a′)
AIE(VIE)		8.59 (8.72)	8.76 (8.80)

[a] AVDZ = Aug-cc-pVDZ.

Table S2. Computed AIE and VIE values (in eV) to the lowest $^2A''$ and $^2A'$ states of $(CH_3)_2COO^+$ from the the $\tilde{X}^1A'$ state of $(CH_3)_2COO$ obtained at higher levels of calculations.

Methods[a]	$^2A''$		$^2A'$	
	AIE	VIE	AIE	VIE
RMP2/VTZ-F12[b]	8.852	8.950	9.016	9.038
RMP2-F12/VTZ-F12	8.968	9.069	9.135	9.159
UCCSD-F12a/VTZ-F12	8.618	8.701	8.777	8.794
UCCSD-F12b/VTZ-F12	8.591	8.674	8.752	8.769
UCCSD(T)-F12a/VTZ-F12	8.845	8.941	8.994	9.016
UCCSD(T)-F12b/VTZ-F12	8.818	8.914	8.969	8.991
RMP2/VQZ-F12	8.916	9.015	9.082	9.105
RMP2-F12/VQZ-F12[c]	8.974	9.075	9.142	9.166
UCCSD-F12a/VQZ-F12	8.616	8.699	8.776	8.793
UCCSD-F12b/VQZ-F12	8.600	8.683	8.761	8.778
UCCSD(T)-F12a/VQZ-F12	8.841	8.937	8.993	9.014
UCCSD(T)-F12b/VQZ-F12	8.825	8.921	8.978	9.000
UCCSD(T)-F12a/CBS[d]	8.838(13)	8.934(13)	8.992(14)	9.013(14)
UCCSD(T)-F12b/CBS[d]	8.831(6)	8.927(6)	8.984(6)	9.006(6)
Best (average of CBS values)[e]	8.835(10)	8.931(10)	8.988(10)	9.010(10)
AIE_0 = Best AIE + ΔZPE[f]	8.79(1)		8.97(1)	

[a] RHF/UCCSD(T)-F12x, x = a or b energy calculations at B3LYP/6-311++G** geometries; see text.

[b] The cc-pVTZ-F12 and cc-pVTZ-F12/OPTRI basis sets designed for F12 calculations were used in the AO and RI basis sets together with the cc-VTZ/JKFIT basis set in the DF basis set. The total number of contracted Gaussian functions in the AO, RI and DF basis sets are 373, 621 and 806, respectively.

[c] The cc-pVQZ-F12 and cc-pVQZ-F12/OPTRI basis sets designed for F12 calculations were used in the AO and RI basis sets together with the cc-VQZ/JKFIT basis set in the DF basis set. The total number of contracted Gaussian functions in the AO, RI and DF basis sets are 639, 730 and 1320, respectively.

[d] The $1/X^3$ formula was employed to obtain the CBS value. Uncertainties are estimated by the differences between the CBS and UCCSD(T)-F12b/VQZ-F12 values.

[e] The best values are estimated by taking the average of the F12a/CBS and F12b/CBS values. Uncertainties are estimated by taking the differences between the best and UCCSD(T)-F12b/VQZ-F12 values.

[f] ΔZPE, zero-point energy corrections, have used the computed B3LYP/6-311++G** harmonic vibrational frequencies.

*Table S3. Optimized geometrical parameters (bond lengths in Å and angle in degrees), computed harmonic vibrational frequencies (in cm^{-1}) of the $\tilde{X}^1A$ state of CH_2=C(CH_3)(OOH) at C_1 and C_S symmetries, and the $\tilde{X}^2A''$ state of CH_2=C(CH_3)$(COOH)^+$ obtained at the B3LYP/6-311++G** level of calculation, and the computed relative electronic energies (ΔE_e in $kcal.mol^{-1}$), and adiabatic (AIE) and vertical (VIE) ionization energies (in eV) obtained at different levels of calculation.*

B3LYP	**Neutral**		**Cation**
	$\tilde{X}^1A$	$^1A'$	$\tilde{X}^2A''$
CC	1.5002	1.5083	1.4841
C=C	1.3312	1.3310	1.4092
CO	1.3798	1.3744	1.3038
OO	1.4490	1.4550	1.4242
CCC	126.9	126.8	124.7
C=CO	125.6	125.4	122.4
COO	111.4	110.3	114.2
OOH	99.6	98.4	100.0
HOOC	-128.2	180.0	180.0
Vib. freq.	135, 142, 165 315, 399, 502 547, 735, 843 859, 923, 965 1022, 1071, 1264 1376, 1404, 1433 1472, 1491, 1718 3034, 3087, 3130 3177, 3273, 3780	170i(a″), 147i(a″), 165(a″) 315(a′), 394(a′), 516(a″) 545(a′), 729(a″), 825(a″) 850(a′), 921(a′), 970(a′) 1014(a′), 1049(a″), 1278(a′) 1390(a′), 1405(a′), 1447(a′) 1485(a″), 1488(a′), 1716(a′) 3045(a′), 3108(a″), 3121(a′) 3173(a′), 3277(a′), 3793(a′)	84(a″), 199(a″), 303(a″) 325(a′), 364(a″), 388(a′) 536(a″), 558(a′), 848(a′) 896(a″), 920(a′), 986(a′) 1024(a″), 1031(a′), 1349(a′) 1375(a′), 1398(a′), 1442(a″) 1467(a′), 1485(a′), 1534(a′) 3024(a′), 3080(a″), 3152(a′) 3166(a′), 3284(a′), 3692(a′)
		ΔE_e/kcal.mol^{-1}	**AIE; VIE (eV)**
B3LYP		1.72	8.56; 8.96
RMP2[a]		1.89	8.858; 9.313
RMP2-F12[a]		1.86	8.938; 9.392
UCCSD-F12a[a]		2.08	8.681; 9.125
UCCSD-F12b[a]		2.09	8.668; 9.113
UCCSD(T)-F12a[a]		1.94	8.772; 9.185
UCCSD(T)-F12b[a]		1.95	8.759; 9.173
RMP2[b]			8.904
RMP2-F12[b]			8.942
UCCSD-F12a[b]			8.683
UCCSD-F12b[b]			8.674
UCCSD(T)-F12a[b]			8.776
UCCSD(T)-F12b[a]			8.767
UCCSD(T)-F12a/CBS[c]			8.779
UCCSD(T)-F12b/CBS[c]			8.773
F12/CBS average[d]			8.776±0.009
AIE_0[e]			8.75±0.01

[a] The cc-pVTZ-F12 AO, cc-pVTZ-F12/OPTRI RI and aug-cc-pVTZ/MP2FIT DF basis sets were used.
[b.] The cc-pVQZ-F12 AO, cc-pVQZ-F12/OPTRI RI and aug-cc-pVQZ/MP2FIT DF basis sets were used.
[c] The $1/X^3$ extrapolation formula was used.
[d] The average of the UCCSD(T)-F12a/CBS and UCCSD(T)-F12b/CBS values. The uncertainty is estimated by the difference between the average CBS and UCCSD(T)-F12b/VQZ-F12 values.
[e] ΔZPE correction from computed B3LYP harmonic vibrational frequencies; the uncertainty includes 10% of ΔZPE.

Table S4. Computed relative energies (in kcal/mol) of the reactions:

$(CH_3)_2CI + O_2 \rightarrow (CH_3)_2CIOO$ …. Reaction 1

$(CH_3)_2CIOO \rightarrow (CH_3)_2COO + I$ …. Reaction 2

obtained at different levels of calculation.

Methods[a]	Reaction 1	Reaction 2	
	ΔE_e^{RX}	$\Delta E_e^{\ddagger}$	ΔE_e^{RX}
M06-2X/AVDZ[b]	-35.42	19.60	14.76 (22.00)[c]
M06-2X/AVDZ[b] ΔE_{0K}	-31.80	18.35	13.74 (20.98)[c]
M06-2X/AVDZ[b] ΔH_{298K}	-32.96	18.42	14.29 (21.53)[c]
RHF/UCCSD/AVTZ[d]	-32.08	26.71	17.77 (25.02)[c]
RHF/UCCSD(T)/AVTZ[d]	-33.75	23.42	17.63 (24.88)[c]
RHF/RMP2/AVTZ[d,e]	-18.66	24.03	17.28 (24.53)[c]
RHF/RMP2-F12/AVTZ[d,e]	-19.60	23.23	15.62 (22.87)[c]
RHF/UCCSD-F12a/AVTZ[d,e]	-32.81	26.65	17.82 (25.07)[c]
RHF/UCCSD-F12b/AVTZ[d,e]	-32.15	26.53	17.67 (24.91)[c]
RHF/UCCSD(T)-F12a/AVTZ[d,e]	-34.34	22.36	17.72 (24.56)[c]
RHF/UCCSD(T)-F12b/AVTZ[d,e]	-34.05	22.62	17.53 (24.78)[c]
Best (average of F12a and F12b)	-34.2	22.5	17.4 (24.7)[c]
Best ΔE_{0K}[f]	-30.6	21.2	16.4 (23.6)
Best ΔH_{298K}	-31.7	21.3	16.9 (24.2)
CASSCF(3,4)/AVDZ[b]		23.14	
CASSCF(3,4)/AVTZ[d]		23.95	
CASSCF(3,4)/NEVPT2/AVDZ[b]		25.58	
CASSCF(3,4)/NEVPT2/AVTZ[d]		23.09	
NEVPT2/CBS[g]		22.05	
CASSCF(3,4)/RSPT2/AVTZ[d]		28.57	
CASSCF(3,4)/RSPT2-F12/AVDZ[b,h]		28.45	
CASSCF(3,4)/RSPT2-F12/AVTZ[d,e]		28.19	
RSPT2-F12/CBS[g]		28.08	

[a] All higher level energy calculations were carried out at M06-2X/AVDZ geometries, and the computed M06-2X/AVDZ harmonic vibrational frequencies were used to evaluate the ZPE and vibrational thermal contributions at 298 K in order to obtain ΔE_{0K} and ΔH_{298K} values, respectively.

[b] Aug-cc-pVDZ basis sets were used for C, O and H, while the aug-cc-pVDZ-PP basis set was used together with the ECP28MDF fully relativistic ECP for I.

[c] For I, spin-orbit (SO) interaction splits the $\tilde{X}^2P$ state to the $^2P_{3/2}$ and $^2P_{1/2}$ states, which has an experimental separation of 7602.97 cm-1 (= 21.738 kcal/mol). In this connection, SO contributions reduce the computed energy of the unperturbed ^2P state by 7.246 kcal/mol to the $^2P_{3/2}$ state. The values given under ΔE_e^{RX} have included SO contributions, while the energies evaluated using the ^2P unperturbed energies for I are in parentheses.

[d] Aug-cc-pVTZ basis sets were used for C, O and H, while the aug-cc-pVTZ-PP basis set was used together with the ECP28MDF fully relativistic ECP for I.

[e] The AO basis sets employed are as in footnote d. For C, O and H, the aug-cc-pVTZ_OPTRI and aug-cc-pVTZ/MP2FIT basis sets are used in the DF and RI basis sets, while for I, the s, p, d and f functions of the def2-ATZVPP-MP2FIT and def2-TZVPP-OPT basis sets were used. The total numbers of contracted Gaussian functions in the AO, RI and DF basis sets are 423, 628 and 884.

[f] ΔZPE correction from computed B3LYP harmonic vibrational frequencies.

[g] The $1/X^3$ formula was employed to obtain the CBS value.

[h] The AO basis sets employed are as in footnote b. For C, O and H, the aug-cc-pVDZ_OPTRI and aug-cc-pVDZ/MP2FIT basis sets are used in the DF and RI basis sets, while for I, the s, p and d functions of the def2-ASVP-MP2FIT and def2-SVP-OPT basis sets were used. The total numbers of contracted Gaussian functions in the AO, RI and DF basis sets are 201, 511 and 682.

Table S5 Computed results on 3-methyl-1,2-dioxetane and its cation.

B3LYP/6-311++G**	Neutral (^{1}A)	Cation (^{2}A)
C_1C_2, C_1O_1, C_2O_2, O_1O_2/Å	1.522, 1.450, 1.463, 1.488	1.534, 1.526, 1.480, 1.337
Vibrational frequencies/cm^{-1}	124, 220, 327, 447, 695, 861, 870, 919, 954, 993, 1098, 1142, 1151, 1197, 1301, 1339, 1400, 1421, 1483, 1495, 1518, 3020, 3025, 3029, 3092, 3096, 3110	171, 234, 325, 440, 674, 773, 857, 916, 921, 997, 1089, 1103, 1169, 1176, 1248, 1315, 1358, 1409, 1461, 1469, 1488, 3037, 3072, 3084, 3109, 3140, 3145
AIE, VIE		8.99, 9.42
At B3LYP geometries	**AIE**	**VIE**
RMP2/VTZ-F12	8.853	8.966
RMP2-F12/VTZ-F12	8.953	9.080
UCCSD-F12a/VTZ-F12	9.138	9.685
UCCSD-F12b/VTZ-F12	9.119	9.666
UCCSD(T)-F12a/VTZ-F12	9.136	9.536
UCCSD(T)-F12b/VTZ-F12	9.117	9.517
Average (F12a/F12b)[a]	9.126 ± 0.010	9.526 ± 0.010
AIE_0 (=AIE + ΔZPE[b])	9.12 ± 0.01	

[a] The uncertainties were estimated by the differences between the averaged F12a and F12b values and the UCCSD(T)-F12a/VTZ-F12 values.

[b] ΔZPE correction from computed B3LYP harmonic vibrational frequencies.

Table S6. Computed results on dimethyl-dioxirane and its cation.

VIE/eV	$^2\mathbf{A_2}$	$^2\mathbf{B_2}$	$^2\mathbf{B_1}$	$^2\mathbf{A_1}$
B3LYP and/or TD-B3LYP/6-311++G**	10.50	11.32	12.46	12.84
CASSCF(8,8)/aug-cc-pVDZ[a]	9.27	11.58	13.16	14.08
CASSCF(8,8)/NEVPT2/aug-cc-pVDZ[a]	10.24	11.74	13.33	15.02
M06-2X/6-311++G ΔE_e/kcal.mol^{-1}**	0.0	32.8	51.3	
$\widetilde{X}^2A_2 \leftarrow \widetilde{X}^1A_1$ ionization[b]	**AIE/eV**	**VIE/eV**		
B3LYP/6-311++G**	9.807	10.504		
RMP2/VTZ-F12	9.555	9.827		
RMP2-F12/VTZ-F12	9.656	9.946		
UCCSD-F12a/VTZ-F12	9.977	10.668		
UCCSD-F12b/VTZ-E12	9.960	10.650		
UCCSD(T)-F12a/VTZ-F12	9.947	10.523		
UCCSD(T)-F12b/VTZ-F12	9.930	10.505		
Average (F12a/F12b)[c]	9.938 ± 0.009	10.514 ± 0.009		
AIE_0 (=AIE + ΔZPE[d])	9.90 ± 0.01			

[a] The axes system is that used in G09 (with the axes system of MOLPRO, b_2 and b_1 swapped). The active space employed consists of the highest doubly occupied and lowest unoccupied orbitals of each irreducible representation (a_1, b_1, b_2 and a_2) of the C_{2V} point group.

[b] At B3LYP/6-311++G** geometries.

[c] The uncertainties were estimated by the differences between the averaged F12a and F12b values and the UCCSD(T)-F12a/VTZ-F12 values.

[d] ΔZPE correction from computed B3LYP harmonic vibrational frequencies.

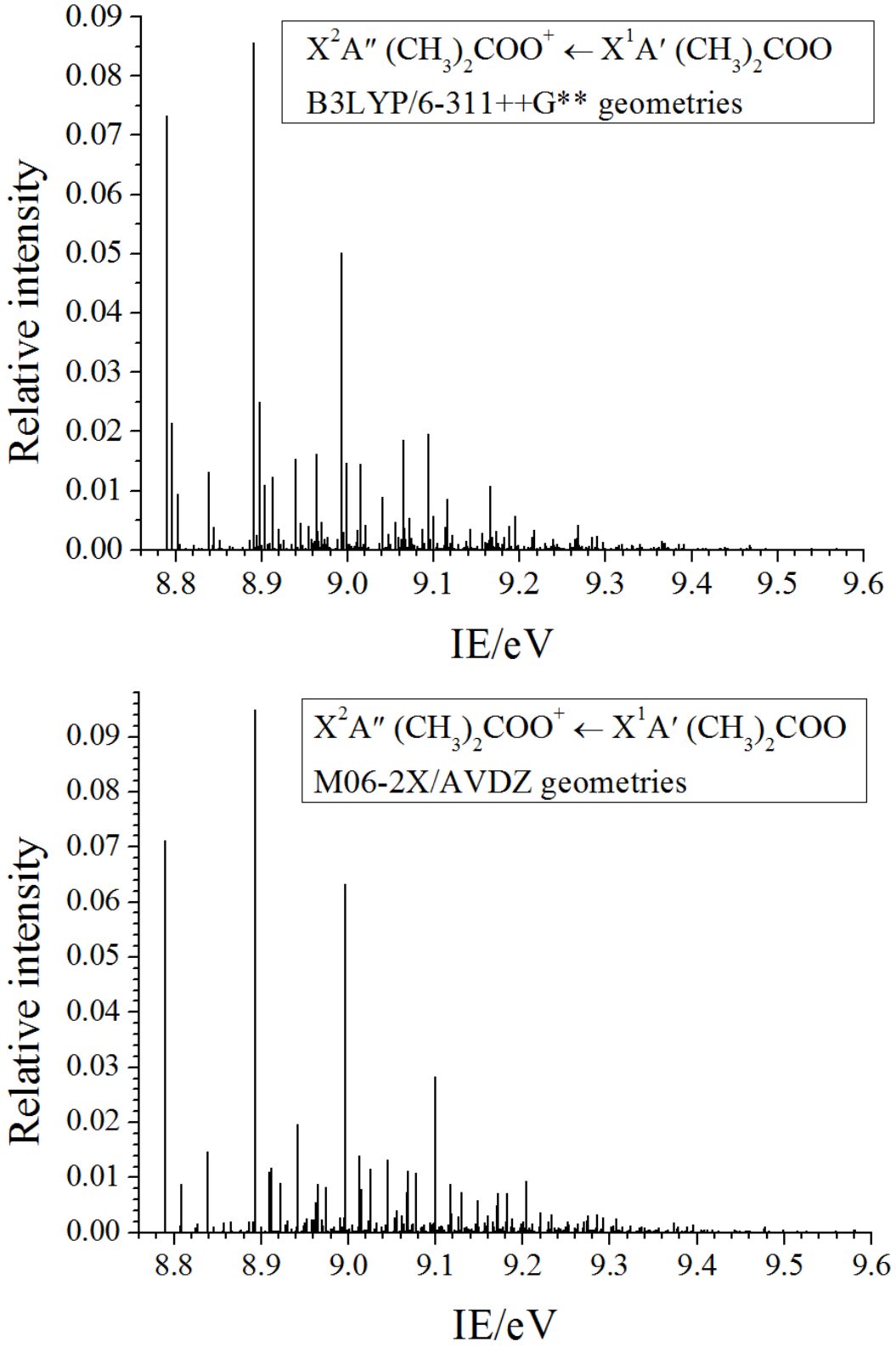

*Figure S1. Computed Franck-Condon factors (FCFs) of the $\tilde{X}^2A''$ $(CH_3)_2COO^+$ ← $\tilde{X}^1A'$ $(CH_3)_2COO$ ionization, obtained using the best computed AIE_0 value of 8.79 eV and the B3LYP/6-311++G** (top bar diagram) and M06-2X/AVDZ (bottom bar diagram) geometries and harmonic vibrational frequencies. The major vibrational progression is the 14a' mode, which is essentially symmetric $(C)_2COO$ skeletal stretching.*

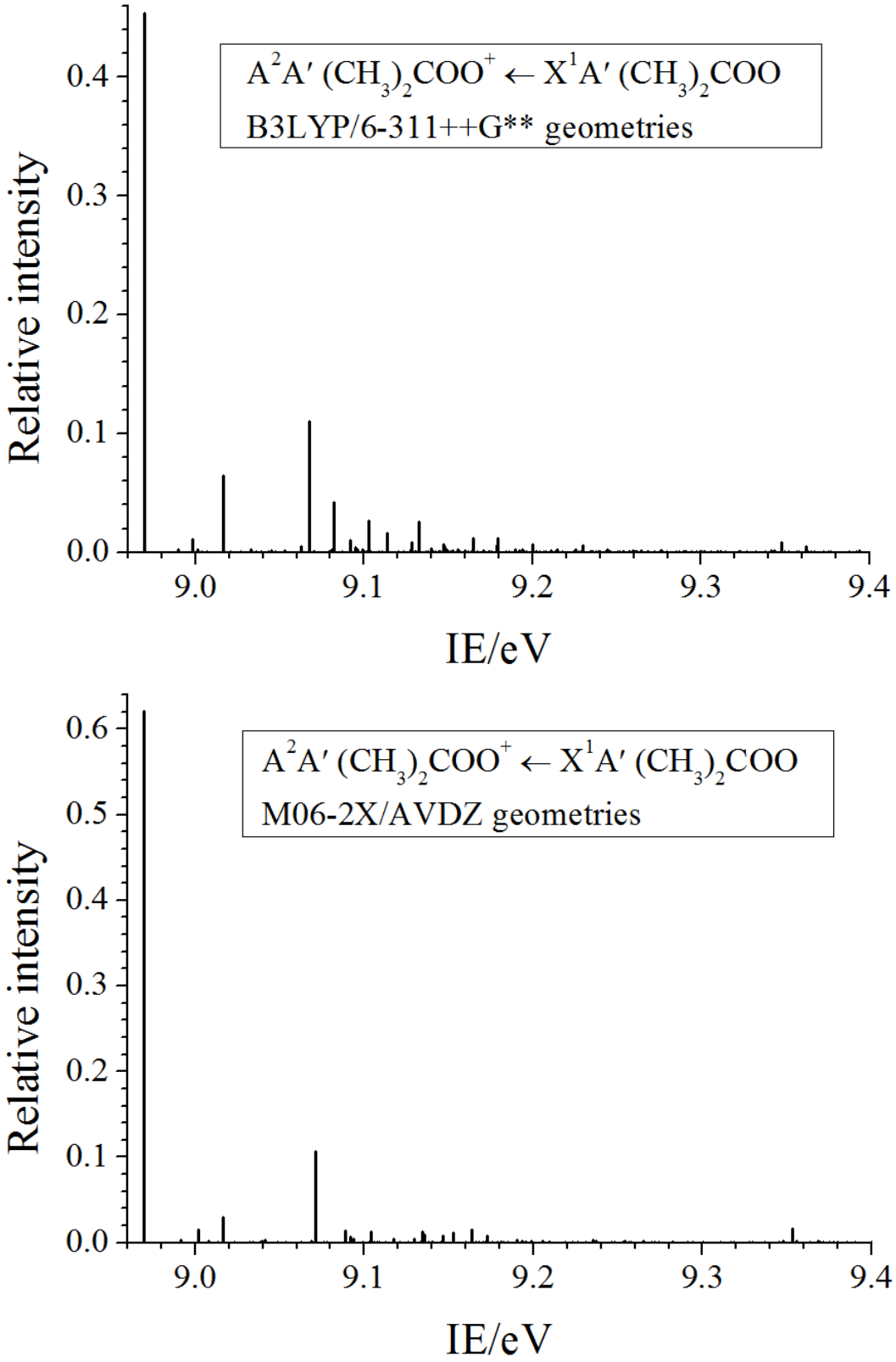

*Figure S2. Computed Franck-Condon factors (FCFs) of the $\tilde{A}^2A'$ $(CH_3)_2COO^+ \leftarrow \tilde{X}^1A'$ $(CH_3)_2COO$ ionization, obtained using the best computed AIE_0 value of 8.97 eV and the B3LYP/6-311++G** (top bar diagram) and M06-2X/AVDZ (bottom bar diagram) geometries and harmonic vibrational frequencies. The major vibrational progression is the 14a′ mode, which is essentially symmetric $(C)_2COO$ skeletal stretching.*

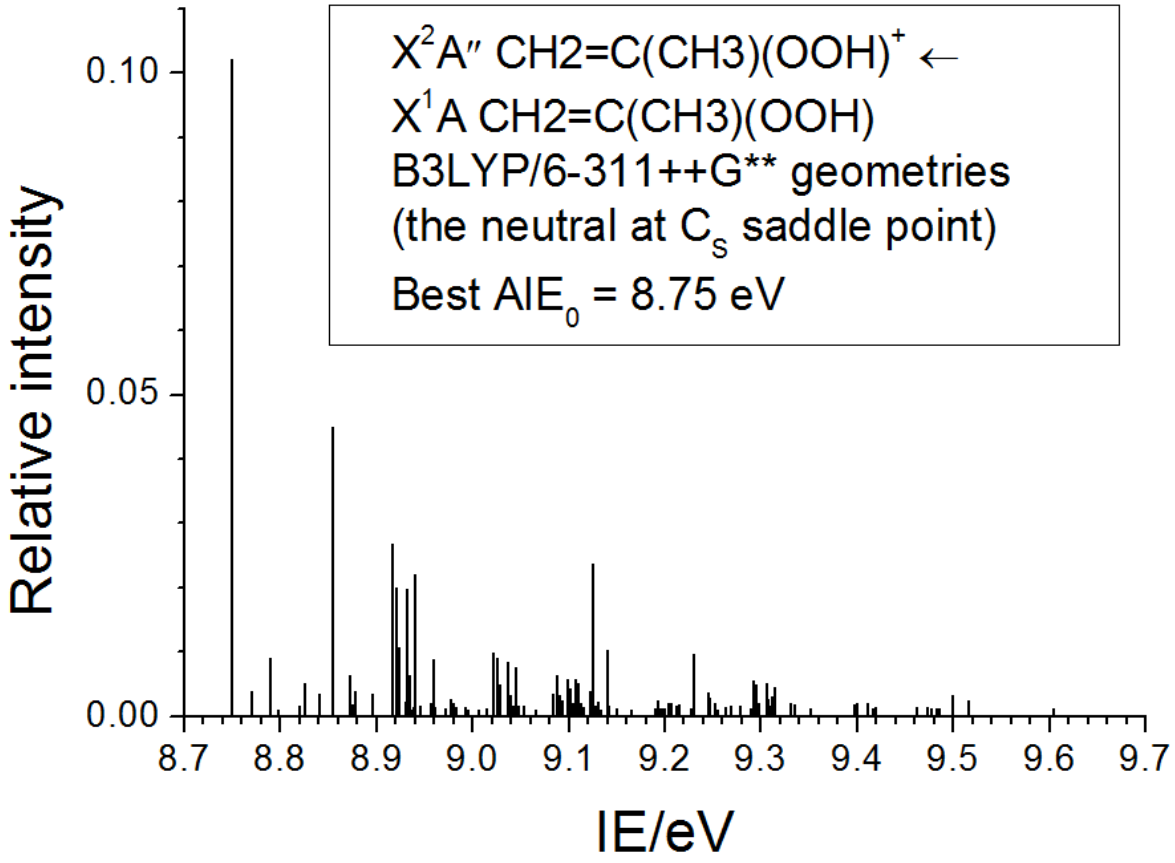

*Figure S3. Computed Franck-Condon factors (FCFs) of the ionization from the $\tilde{X}^1A$ state of CH_2=C(CH_3)(OOH) (at the C_S saddle point; see text) to the $\tilde{X}^2A''$ state of CH_2=C(CH_3)$(OOH)^+$, using the best computed AIE_0 value of 8.75 eV and the B3LYP/6-311++G** geometries and harmonic vibrational frequencies. The major vibrational progression is the 15a' mode, which is essentially symmetric $(C)_2COO$ skeletal stretching.*

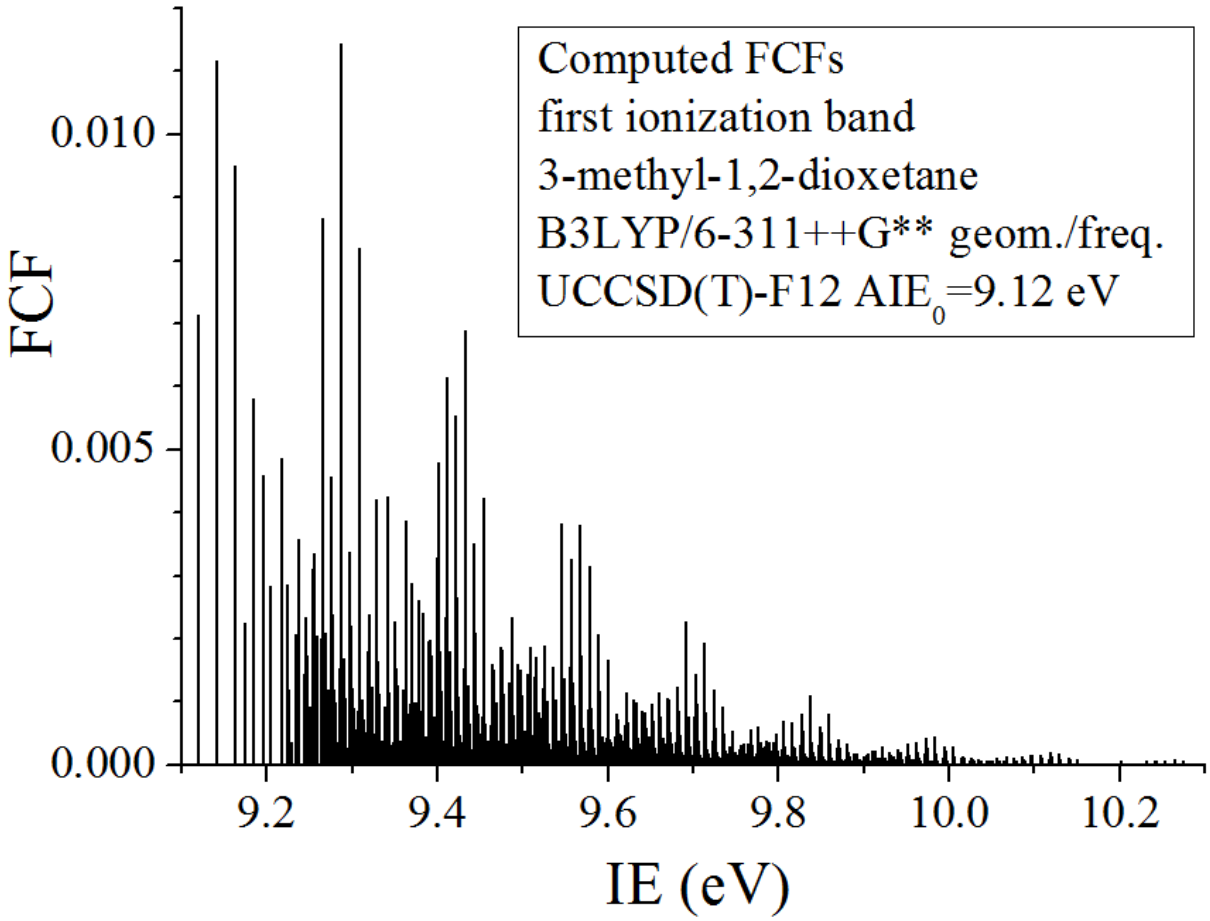

*Figure S4. Computed Franck-Condon factors (FCFs) of the ionization from the $\tilde{X}^1A$ state of 3-methyl-1,2-dioxetane, $CH_3CH(O_2)CH_2$ (CCOO four-membered ring), to the $\tilde{X}^2A$ state of its cation, using the best computed AIE_0 value of 9.12 eV and the B3LYP/6-311++G** geometries and harmonic vibrational frequencies. The major vibrational progressions are the 14a and 27a modes with computed frequencies of 171 and 1176 cm^{-1}, which are essentially the methyl-ring wagging mode and bond stretches in the CCOO four-membered ring.*

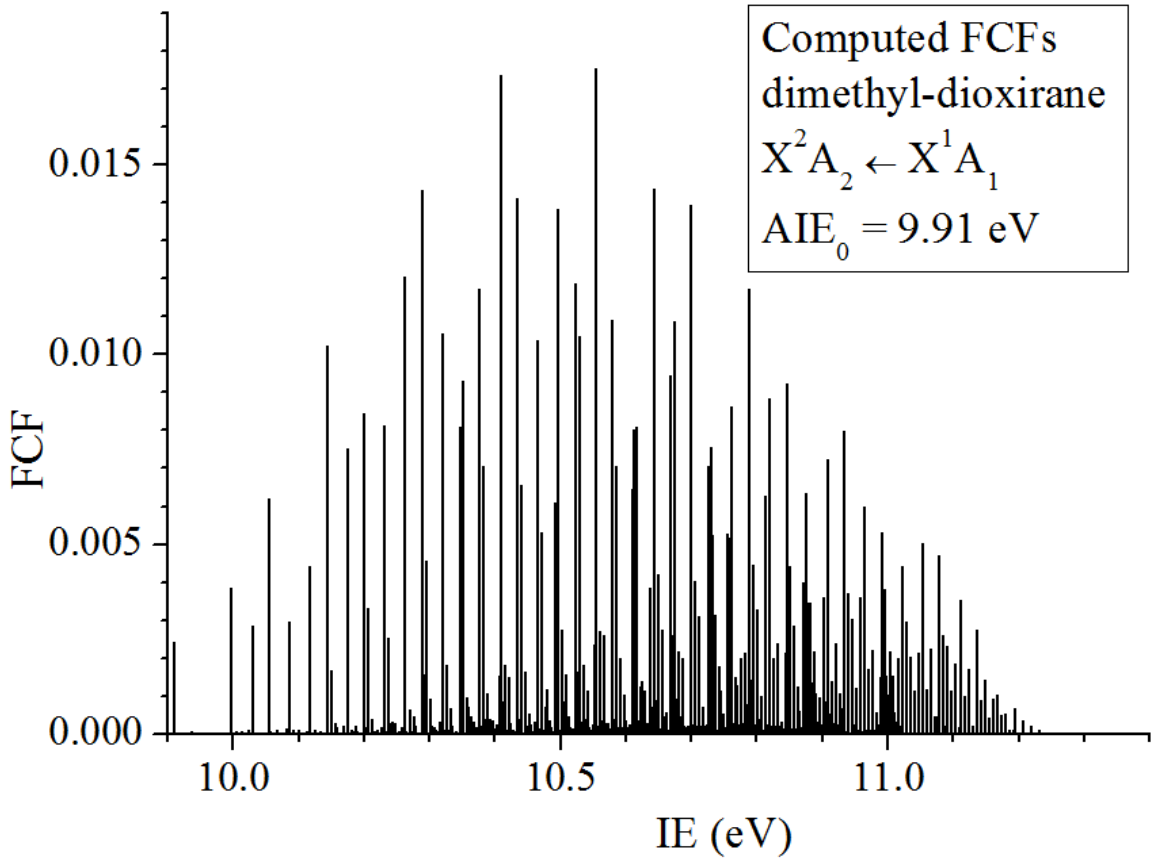

*Figure S5. Computed Franck-Condon factors (FCFs) of the ionization from the $\widetilde{X}^1A_1$ state of dimethyl-dioxirane, $CH_3C(O_2)CH_3$ (COO three-membered ring), to the $\widetilde{X}^2A_2$ state of its cation, using the best computed AIE_0 value of 9.91 eV and the B3LYP/6-311++G** geometries and harmonic vibrational frequencies.*

$(CH_3)_2CI_2$ σ_{355nm}

Absorption cross section of $(CH_3)_2CI_2$ at 355nm was obtained by using the absorption cross section of CH_2I_2 as a reference. Figure S6 shows the change in ring-down time due to addition of different concentrations of $(CH_3)_2CI_2$ and CH_2I_2. Gas flows similar to the 10 Torr experiments for characterization of $(CH_3)_2COO$ self-reaction and unimolecular reaction rates were used to obtain these measurements.

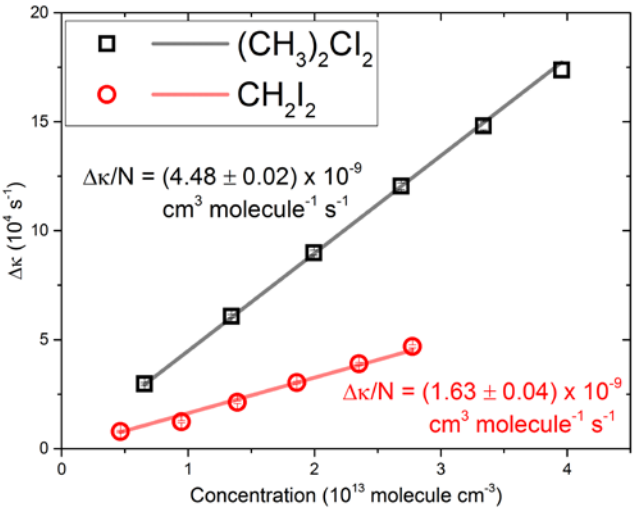

Figure S6 Change in ring-down rate due to addition of different concentrations of $(CH_3)_2CI_2$ and CH_2I_2. The solid line shows the linear fit and the slope is related to absorption cross section of the absorbing species.

The change in the ring-down rate with and without absorbing species is given by

$$\Delta\kappa = \frac{\sigma N c l}{L} \qquad \text{(S1)}$$

where l is the sample pathlength within the cavity. All the other symbols represent the same parameters as described in the main text. Using equation (S1), absorption cross section of $(CH_3)_2CI_2$ is given by

$$\sigma_{355nm,\,(CH_3)_2CI_2)} = \left(\frac{\Delta\kappa_{\,(CH_3)_2CI_2)}}{N_{\,(CH_3)_2CI_2)}}\right)\left(\frac{\Delta\kappa_{CH_2I_2}}{N_{CH_2I_2}}\right)^{-1} \sigma_{355nm,\ \ CH_2I_2} \qquad \text{(S2)}$$

Using the absorption cross section value of CH_2I_2, $\sigma_{355nm,\ \ CH_2I_2}$ = (1.92 ± 0.23) x 10^{-19} cm^2,[19] and the slope values from Figure S6, absorption cross section of $(CH_3)_2CI_2$, $\sigma_{355nm,\,(CH_3)_2CI_2)}$, was found to be (5.75 ± 0.74) x 10^{-19} cm^2. This value was used to find the fractional depletion of $(CH_3)_2CI_2$ precursor molecules as described in the main text.

$(CH_3)_2CI_2$ depletion

The change in ring down rate with and without photolysis laser is given by

$$\Delta\kappa = \frac{1}{\tau_{on}} - \frac{1}{\tau_{off}} = \left[\frac{N^0 c(l-d)\sigma_{355nm}}{L} + \frac{Ncd\sigma_{355nm}}{L}\right] - \frac{N^0 cl\sigma_{355nm}}{L} \qquad \text{(S3)}$$

. Here τ is the ring-down time, l is the sample length within the cavity and all the other symbols represent the same parameters as described in the main text. The precursor concentration in the overlap length region, d, are expected to decrease due to photolysis and result in the depletion of the precursor signal. Equation S3 can be rearranged to give equation (6) shown in the main text.

$(CH_3)_2COO$ self-reaction and unimolecular reaction

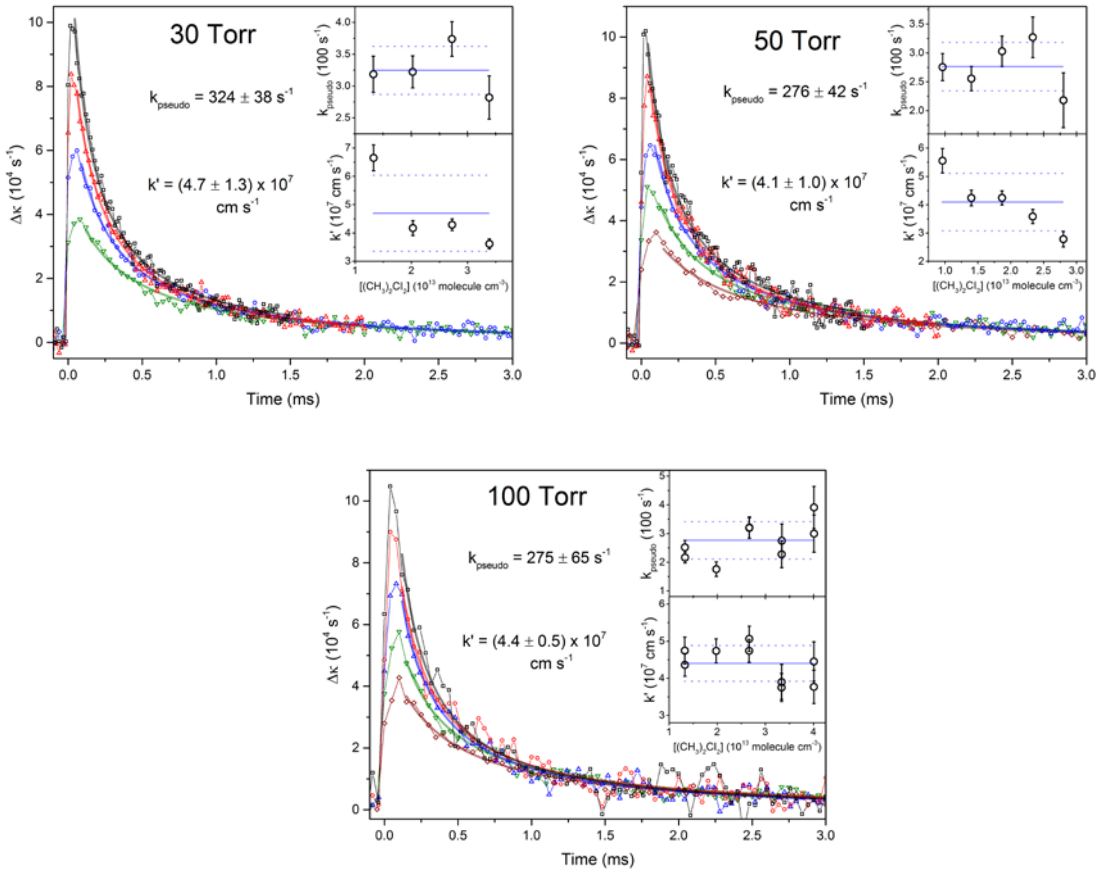

Figure S7 $(CH_3)_2COO$ decay rate coefficients as a function of $(CH_3)_2Cl_2$ precursor concentration at 30, 50 and 100 Torr total pressure. In the pressure-dependence studies, the partial pressure of N_2 was increased, whereas the O_2 and $(CH_3)_2Cl_2$ pressures were kept constant. The solid lines show the fits to the decay traces using equation (3). The top and bottom insets in each panel show the k_{pseudo} and k' values obtained from the fits for different $(CH_3)_2Cl_2$ concentrations.

.

Figure S7 shows the $(CH_3)_2COO$ decay traces obtained at different precursor concentrations and at different total pressures. The fit procedure is described in detail in the main text. All the k_{pseudo} rate coefficient values obtained at different total pressures are within the bound of uncertainties of the measurements.

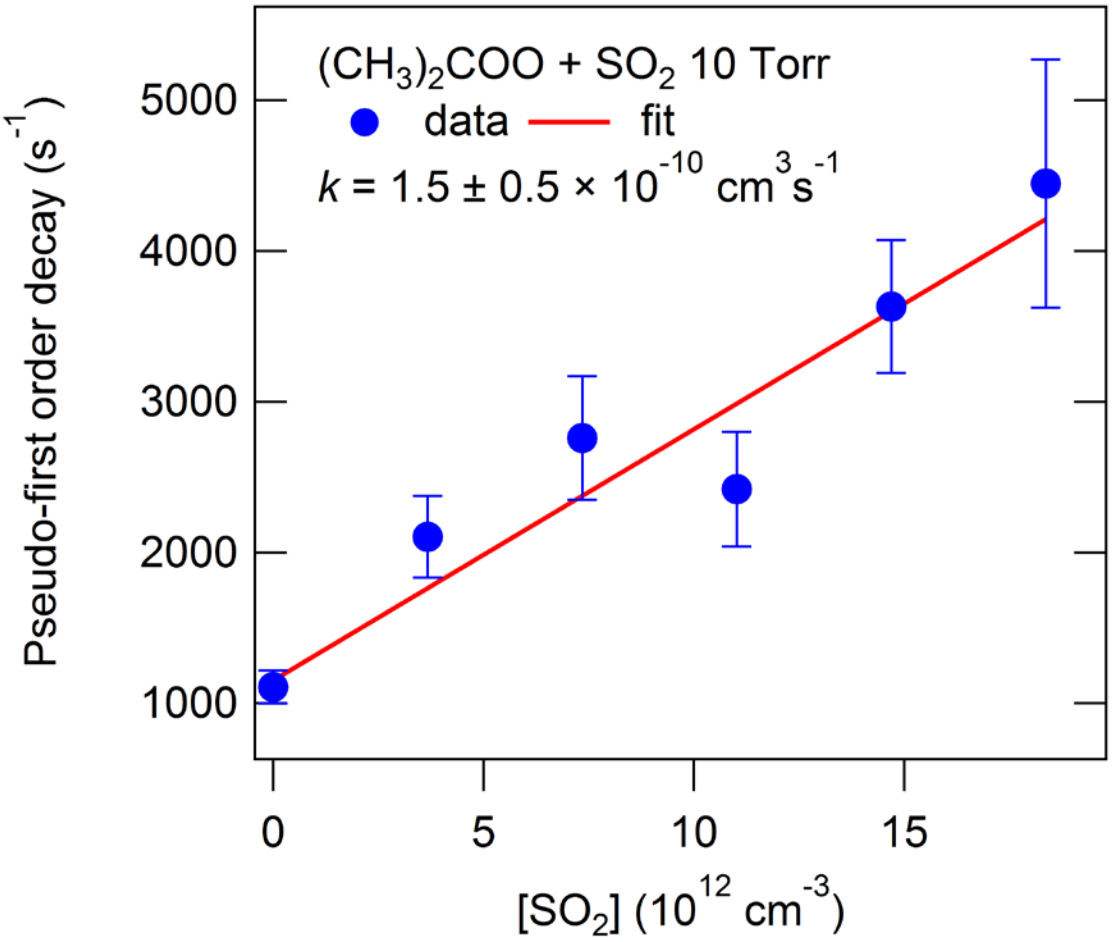

Figure S8. Plot of measured pseudo-first order decay constant for acetone oxide as a function of [SO_2], taken at 10 Torr total pressure (He buffer).

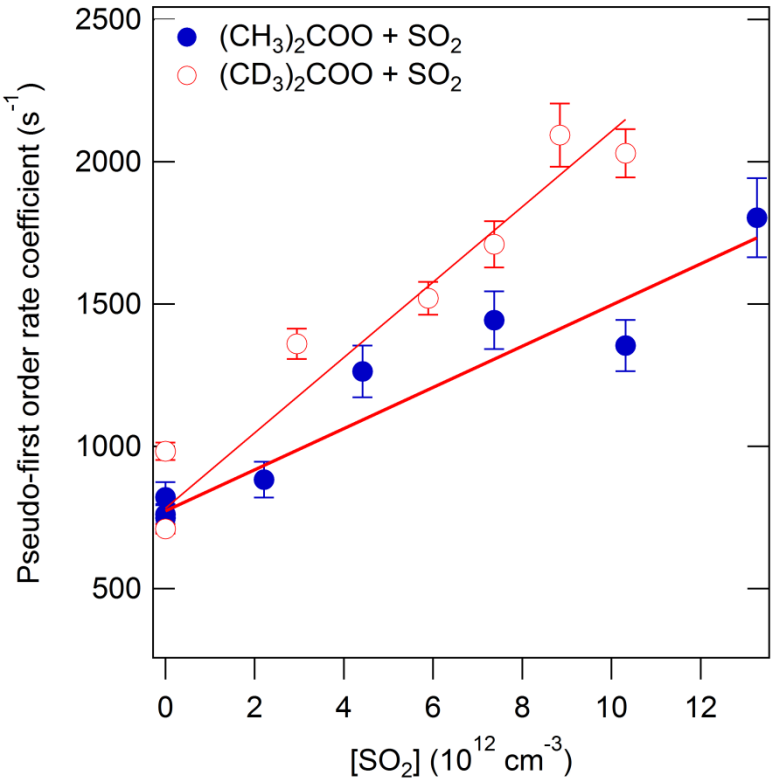

Figure S9. Deuterium isotope effect for the reaction of acetone oxide with SO_2 at 4 Torr total pressure (He buffer)

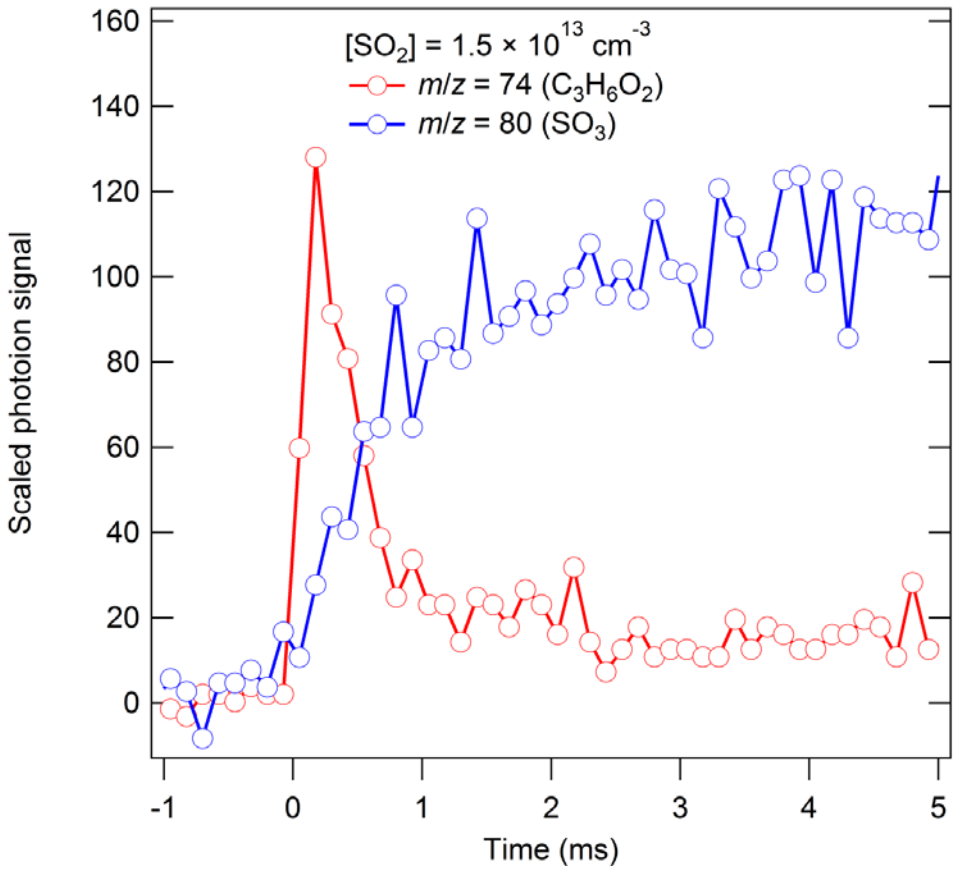

Figure S10. Comparison of the rise of SO_3 product with the decay of acetone oxide reactant in the presence of SO_2. The time constants are similar.

References

1. Knizia, G.; Adler, T. B.; Werner, H.-J., *J. Chem. Phys.* **2009,** *130*, 054104.
2. Werner, H.-J.; Knowles, P. J.; Manby, F. R.; Schütz, M.; Celani, P.; Knizia, G.; Korona, T.; Lindh, R.; Mitrushenkov, A.; Rauhut, G.; Adler, T. B.; Amos, R. D.; Bernhardsson, A.; Berning, A.; Cooper, D. L.; Deegan, M. J. O.; Dobbyn, A. J.; Eckert, F.; Goll, E.; Hampel, C.; Hesselmann, A.; Hetzer, G.; Hrenar, T.; Jansen, G.; Köppl, C.; Liu, Y.; Lloyd, A. W.; Mata, R. A.; May, A. J.; McNicholas, S. J.; Meyer, W.; Mura, M. E.; Nicklass, A.; Palmieri, P.; Pflüger, K.; Pitzer, R.; Reiher, M.; Shiozaki, T.; Stoll, H.; Stone, A. J.; Tarroni, R.; Thorsteinsson, T.; Wang, M.; Wolf, A. *MOLPRO, version 2012.1, a package of ab initio programs (see http://www.molpro.net).* 2012.
3. Peterson, K. A.; Thomas B. Adler; Werner, H.-J., *J. Chem. Phys.* **2008,** *128*, 084102.
4. Hill, J. G.; Mazumder, S.; Peterson, K. A., *J. Chem. Phys.* **2010,** *132*, 054108.
5. Yousaf, K. E.; Peterson, K. A., *Chem. Phys. Lett.* **2009,** *476* (4-6), 303-307.
6. Weigend, F.; Köhn, A.; Hättig, C., *J. Chem. Phys.* **2002,** *116*, 3175-3183.
7. Mozhayskiy, A.; Krylov, A. I. *ezSpectrum, http://iopenshell.usc.edu/downloads; this work was conducted using the resources of the iOpenShell Center for Computational Studies of Electronic Structure and Spectroscopy of Open-Shell and Electronically Excited Species (http://iopenshell.usc.edu) supported by the National Science Foundation through the CRIF:CRF program.*
8. Frisch, M. J.; Trucks, G. W.; Schlegel, H. B.; Scuseria, G. E.; Robb, M. A.; Cheeseman, J. R.; Scalmani, G.; Barone, V.; Mennucci, B.; Petersson, G. A.; Nakatsuji, H.; Caricato, M.; Li, X.; Hratchian, H. P.; Izmaylov, A. F.; Bloino, J.; Zheng, G.; Sonnenberg, J. L.; Hada, M.; Ehara, M.; Toyota, K.; Fukuda, R.; Hasegawa, J.; Ishida, M.; Nakajima, T.; Honda, Y.; Kitao, O.; Nakai, H.; Vreven, T.; Montgomery, J., J. A.; Peralta, J. E.; Ogliaro, F.; Bearpark, M.; Heyd, J. J.; Brothers, E.; Kudin, K. N.; Staroverov, V. N.; Kobayashi, R.; Normand, J.; Raghavachari, K.; Rendell, A.; Burant, J. C.; Iyengar, S. S.; Tomasi, J.; Cossi, M.; Rega, N.; Millam, N. J.; Klene, M.; Knox, J. E.; Cross, J. B.; Bakken, V.; Adamo, C.; Jaramillo, J.; Gomperts, R.; Stratmann, R. E.; Yazyev, O.; Austin, A. J.; Cammi, R.; Pomelli, C.; Ochterski, J. W.; Martin, R. L.; Morokuma, K.; Zakrzewski, V. G.; Voth, G. A.; Salvador, P.; Dannenberg, J. J.; Dapprich, S.; Daniels, A. D.; Farkas, Ö.; Foresman, J. B.; Ortiz, J. V.; Cioslowski, J.; Fox, D. J. *Gaussian 09, Revision A.02*, Gaussian, Inc.: Wallingford CT, 2009.
9. Watts, J. D.; Gauss, J.; Bartlett, R. J.; 10.1063/1.464480, *J. Chem. Phys.* **1993,** *98* (11), 8718-8733.
10. Angeli, C.; Cimiraglia, R.; Evangelisti, S.; Leininger, T.; Malrieu, J. P., *Journal of Chemical Physics* **2001,** *114* (23), 10252-10264.
11. Angeli, C.; Cimiraglia, R.; Malrieu, J. P., *Journal of Chemical Physics* **2002,** *117* (20), 9138-9153.
12. Angeli, C.; Pastore, M.; Cimiraglia, R., *Theoretical Chemistry Accounts* **2007,** *117* (5-6), 743-754.
13. Werner, H.-J., *Mol. Phys.* **1996,** *89* (2), 645-661.
14. Shiozaki, T.; Werner, H.-J., *J. Chem. Phys.* **2010,** *133*, 141103
15. Weigend, F.; Ahlrichs, R., *Phys. Chem. Chem. Phys.* **2005,** *7*, 3297-3305.
16. Knizia, G. Explicitly correlated quantum chemistry methods for high-spin open-shell molecules. Universität Stuttgart, 2010.
17. Bischoff, F. A.; Wolfsegger, S.; Tew, D. P.; Klopper, W., *Mol. Phys.* **2009,** *107* (8-12), 963-975.
18. Lee, E. P. F.; Mok, D. K. W.; Shallcross, D. E.; Percival, C. J.; Osborn, D. L.; Taatjes, C. A.; Dyke, J. M., *Chem.-Eur. J.* **2012,** *18* (39), 12411-12423.
19. Mössinger, J. C.; Shallcross, D. E.; Cox, R. A., *J. Chem. Soc., Faraday Trans.* **1998,** *94*, 1391-1396.